crystals

MDPI

Article

Results from exploratory work in Li-rich regions of the *AE*-Li-Ge systems (*AE* = Ca, Sr, Ba)

Jiliang Zhang [1,2] and Svilen Bobev [1,*]

[1] Department of Chemistry & Biochemistry, University of Delaware, Newark, DE 19716, USA
[2] School of Materials Science and Engineering, Dalian Jiaotong University, Dalian 116028, P.R. China
* Correspondence: Email: bobev@udel.edu; Telephone: +1-302-831-8720; Fax: +1-302-831-6335

Abstract: The compounds *AE*Li_2Ge (*AE* = Ca, Sr and Ba) were synthesized and their structures were determined as a part of the exploratory work in the Li-rich regions of the respective ternary systems. The three compounds are isostructural and their crystal structure is the analogous with the orthorhombic structure of $BaLi_2Si$ and KLi_2As (space group *Pmmn*). The atomic arrangement can be viewed as an intergrowth of corrugated *AE*Ge layers, alternated with slabs of Li atoms, suggestive of the possible application of these phase as electrode materials for lithium-ion batteries. Both experimental electronic density and calculated electronic structure suggest that the valence electrons can be partitioned as $(AE^{2+})(Li^{+})_2(Ge^{4-})$, i.e., the title compounds are valence precise Zintl phases. The band structure calculations for $BaLi_2Ge$ show that a bona-fide energy gas in the band structure does not exist, and that the expected poor metallic behavior is originated from the *AE*Ge layer and related to hybridization of Ba5*d* and Ge3*p* states. In addition, electrochemical measurements indicate that Li atoms can be intercalated into CaGe with a maximum capacity of 446 mAh/g, and reveal the possibility of the hitherto unknown CaLiGe to exist as a metastable phase.

Keywords: crystal structure; germanium, lithium; X-ray diffraction, Zintl phases

1. Introduction

Despite the huge investment and extensive studies in the technology of Lithium-ion batteries (LIB), the development of LIB still lags far behind the requirement of many electric devices. Most popular electrodes are still based on materials proposed many years ago [1–3], like $LiCoO_2$ for cathode and graphite for anode. Many current investigations are still focused on improving the properties of these materials [4–6]. One of the main reasons for this is the lack of an effective guideline/way for the discovery of new materials as high-performance electrodes and many breakthroughs are serendipitous. Modern developments for materials discovery call for the use of density functional theory (DFT) calculations, which predict mainly the most stable structure in the systems [7,8]. Such calculations generally take huge amounts of time and may have difficulties identifying structures with energy of local minimum. Another drawback is the fact that the routine calculation does not take into the account the required compositions and functions. Another complication is arising

Citation: To be added by editorial staff during production.

Academic Editor: Firstname Lastname

Received: date
Revised: date
Accepted: date
Published: date

from the fact that many Li-containing compounds are sensitive to air and/or moisture, greatly hindering the experimental work. As rule, the lower the concentration of Li in a compound, the more stable the compound is with respect to oxidation by air [9,10]. Thus, it is difficult to explore phase space for Li-rich compounds.

Since the subjects of this paper are germanides, we can make a case in point by recapping some oddities in the Li–Ge system [11]. For example, years ago, there was a reported "Li_3Ge" phase that even today is not reconciled with the crystallograhically characterized Li_5Ge_2 (or the nearby Li_7Ge_2, re-assigned as $Li_{13}Ge_4$ and Li_9Ge_4, the structures of which are not well established to date [12,13]). The previously reported "Li_4Ge" turns out to be compositionally closest to the compound $Li_{4.1}Ge$ [14], and not $Li_{15}Ge_4$ [15] or $Li_{17}Ge_4$ [14] (the latter has also been referred to as $Li_{21}Ge_5$ or $Li_{22}Ge_5$ in the older literature [16]). When considering ternary systems, a multitude of Li germanides is reported, but very few of them are Li-rich [17,18]. It is also the case in ternary systems containing Li and elements of group 15 [19,20]. It is already realized that many compounds containing group 14 or 15 elements and metallic elements especially alkali and alkaline-earth metals are Zintl phases [21–23]. In Zintl phases, there exists a well-defined relationship between chemical and electronic structures [24]. Therefore, using the Zintl concept as a guideline, it should be possible to accelerate the discovery of new materials.

With this paper we report on the compounds $AELi_2Ge$ (*AE* = Ca, Sr and Ba), which were obtained via our exploratory work in the Li-rich regions of the respective ternary systems. While this research was ongoing, another team published the structures of $CaLi_2Ge$ and $BaLi_2Ge$ [25], leaving $SrLi_2Ge$ as the only new compound covered in this report. We still report the refinements of the structures of $CaLi_2Ge$ and $BaLi_2Ge$ because our crystallographic analysis is not done at ambient temperature and comparing the metrics of the three structure can be instructive.

2. Materials and Methods

2.1. Synthesis

Handling of the starting materials [pure elements from Alfa or Aldrich (>99.9 wt%)] was performed inside an argon-filled glovebox or under vacuum. Ba and Ge are used as received. The surface of Li metal had to be carefully cleaned with a blade every time the metal rod was cut. In a typical experiment, a mixture of constituent elements with stoichiometric compositions were loaded into a Nb tube, which was then sealed by arc-welding under an Ar atmosphere. The welded tube was transfered into a high-frequency induction melter and the containing materials were melted at ca. 1000 °C for 3 minutes. Subsequently the Nb tube with the melt inside was cooled, taken out and placed inside a fused silica tube, which was then sealed under vacuum. The assembly was heated in a muffle furnace to temperature of 800 °C (rate of 1 °/min) and equilibrated

for 7 days, followed by air cooling to room temperature. The synthesized samples are air sensitive and the colour changes from silver to light brown in hours upon exposure to ambient atmosphere.

2.2. Crystallographic analysis

Powder X-ray diffraction data were collected at room temperature using a Rigaku MiniFlex powder diffractometer (Cu *K*α radiation) which was enclosed and operated inside a nitrogen-filled glovebox to measure air sensitive samples. The main reflections cannot be matched with known compounds involved in the systems and their oxides, indicating the formation of a new phase. Indexing on the main reflections yield a primitive orthorhombic unit cell.

Table 1. Selected Crystallographic Data for *AE*Li_2Ge (*AE*=Ca, Sr, Ba).

CCDC number	2314734	2314735	2314736
Empirical formula	$CaLi_2Ge$	$SrLi_2Ge$	$BaLi_2Ge$
Formula weight	126.55	174.09	223.81
Temperature		200(2) K	
Radiation, λ		Mo *K*α, 0.71073 Å	
Space group		*Pmmn* (no. 59), *Z* = 2	
Lattice constants			
a/ Å	4.650(2)	4.6818(7)	4.7092(9)
b/ Å	5.766(3)	6.2829(6)	6.7593(9)
c/ Å	6.364(3)	6.2800(7)	6.2923(7)
V/ $Å^3$	170.65(13)	184.81(4)	200.3(1)
ρ/ $g \cdot cm^{-3}$	2.46	3.13	3.60
μ/ cm^{-1}	101.7	222. 8	170.1
R_1 ($I>2\sigma_{(I)}$) [1]	0.0266	0.009	0.0104
wR_2 ($I>2\sigma_{(I)}$) [1]	0.0544	0.0209	0.0201
R_1 (all data) [1]	0.0332	0.0094	0.0114
wR_2 (all data) [1]	0.0566	0.021	0.0268
Largest diff. peak/hole	0.55/–0.67	0.38/–0.32	0.41/–0.51

[1] $R_1 = \sum||F_o| - |F_c||/\sum|F_o|$; $wR_2 = [\sum[w(F_o^2 - F_c^2)^2]/\sum[w(F_o^2)^2]]^{1/2}$, where $w = 1/[\sigma^2F_o^2 + (A \cdot P)^2 + (B \cdot P)]$, and $P = (F_o^2 + 2F_c^2)/3$; A and B are the respective weight coefficients.

Single crystals of *AE*Li_2Ge were selected from the reaction products after breaking the annealed ingots and mounted on the top of glass fibers using Paratone N oil. Intensity data sets were collected at 200 K on a Bruker SMART CCD-diffractometer quipped with monochromated Mo *K*α radiation (λ = 0.71073 Å). The data collection routine in SMART [26] with scans at different angles allowed for full coverage of the reciprocal space up to $2\theta \approx$ 57-58°. The collected frames were integrated using the SAINT package [27]. Semiempirical absorption correction was applied

using SADABS [28]. The structures were solved by direct methods and refined on F^2 with the aid of the SHELXTL package [29]. The final difference Fourier maps were flat with highest maxima and minima not larger than 0.5–0.7 e/Å^3. This, together with the excellent crystallographic parameters (Tables 1 and 2), is suggestive of the fact that all structures are devoid of disorder. The experimental electron density was reconstructed by maximum-entropy method (MEM) using a Dysnomia program [30] and visualized with the VESTA 3 program [31].

Table 2. Atomic Coordinates and Equivalent Isotropic Displacement Parameters (U_{eq})[1] of *AE*Li$_2$Ge (*AE* = Ca, Sr, Ba).

Atom	Site	*x*	*y*	*z*	U_{eq} (Å)
			CaLi$_2$Ge		
Ca	2*b*	1/4	1/4	0.0678(3)	0.0135(4)
Ge	2*b*	1/4	3/4	0.2582(2)	0.0123(3)
Li	4*e*	0	0.0251(15)	0.6018(15)	0.023(2)
			SrLi$_2$Ge		
Sr	2*b*	1/4	1/4	0.0885(1)	0.0108(2)
Ge	2*b*	1/4	3/4	0.2793(1)	0.0102(2)
Li	4*e*	0	0.0369(7)	0.5991(6)	0.0169(8)
			BaLi$_2$Ge		
Ba	2*b*	1/4	1/4	0.0981(1)	0.0126(2)
Ge	2*b*	1/4	3/4	0.3027(2)	0.0110(2)
Li	4*e*	0	0.0483(8)	0.5935(8)	0.016(1)

[1] U_{eq} is defined as one-third of the trace of the orthogonalized U^{ij} tensor.

2.3. Elemental Analysis

Picked single crystals were mounted on to carbon tape and placed in a JEOL 7400 F electron microscope equipped with an INCA-Oxford energy-dispersive spectrometer. The microscope was operated at 10 μA bean current at 15 kV accelerating potential. Data were acquired for several spots on the same crystal and average. The obtained results are in good agreement with the refined compositions (e.g. Ca:Ge ≈ 1:1) and the elemental-mapping confirms the homogeneity of the samples. The Li contents were measured using a Spectro Ciros ICP_OES radia view instrument. Generally 5 mg of product powders were dissolved using a dilute nitric acid (5 mL). All results gave Li contents close to 50%.

2.4. Electronic Structure Calculations

To optimize the geometry of the tetrahedral chains carved out from the BaLi$_2$Ge structure, see the structure description in section 3), a triclinic unit cell containing only one such unit was constructed first. One direction of the unit cell is chosen to be along the propogation of the chains with a

lattice constant equivalent to the Ba—Ba distance in one cluster, while in other directions the initial lattice constants are 1 nm to ensure the isolation of the individual chains. Structural optimizations were performed were performed with the first-principles pseudopotential based density functional theory as implemented in SIESTA [32,33], which employs a localized orbital basis in the representation of wave functions. We use soft norm-conserving pseudopotential and the Perdew-Berke-Emzerhof exchange correlation energy within the generalized gradient approximation [34,35]. The optimizations are deemed to have sufficiently converged when the residual forces on any atoms are smaller than 0.001 eV/Å.

Electronic structure calculations were carried out on the optimized and experimentally determined structures using the projector augmented wave method (APW) with spin orbit coupling (SOC) [36,37]. The Kinetic energy cur-off for the plane waves was 500 eV. Exchange and correlations were treated in the local density approximation (LDA) [38]. For these calculations, an 8×12×12 *k*-point Monkhorst-pack grid was used.

2.5. Electrochemical Measurements

The fine powders of *AE*Li_2Ge compounds are very air sensitive and can be used directly for electrodes. Instead, CaGe fine powders (see the appendix for details on the preparation) were used for electrochemical measurements, because that $CaLi_2Ge$ was expected to be the product from lithiation of CaGe. The CaGe electrodes were prepared by coating slurries containing the active materials (70 wt%), super P carbon conductive agents (20 wt%), and a binder (polyvinylidenedifluoride, 10 wt%), dissolved in N-Mehyl-2-pyrrolidone. The resulting slurries were cast onto a cupper foil current collector and then dried in a vacuum oven at 120 °C for 5 hours. After drying, the electrodes were punched into a coin shape of 12 mm diameter. The electrochemical performance was evaluated using CR2032 coin-type cells assembled in an Ar-filled glovebox. Li metal foil was used as a counter electrode and a 1 M solution in EC/DEC (1:1, v/v) was employed as an electrolyte.

3. Results and Discusion

3.1. Crystal Structure

During the process of electrochemical tests and manuscript preparation, $CaLi_2Ge$ and $BaLi_2Ge$ were synthesized from Li flux, and their structures were reported by another research team [25]. The structure refinements at 200 K we provide here (Table 1) are in excellent agreement with the reported ones [25]. Comparing structural parameters reported at ambient temperature with the present results show that the $CaLi_2Ge$ crystal exhibits a very small thermal expansion: *a* and *c* are almost constant from 200 K to room temperature (4.650(2) Å vs 4.6498(3) Å and

6.364(3) Å vs 6.3683(4) Å), while in $BaLi_2Ge$ the thermal expansion is relatively larger along *a* axis (4.7092(9) Å vs 4.7141(2) Å) and smaller or non-existent along *b* and *c* axes, respectively (6.7593(9) Å vs 6.7655(3) Å, and 6.2923(7) Å vs 6.3042(3) Å).

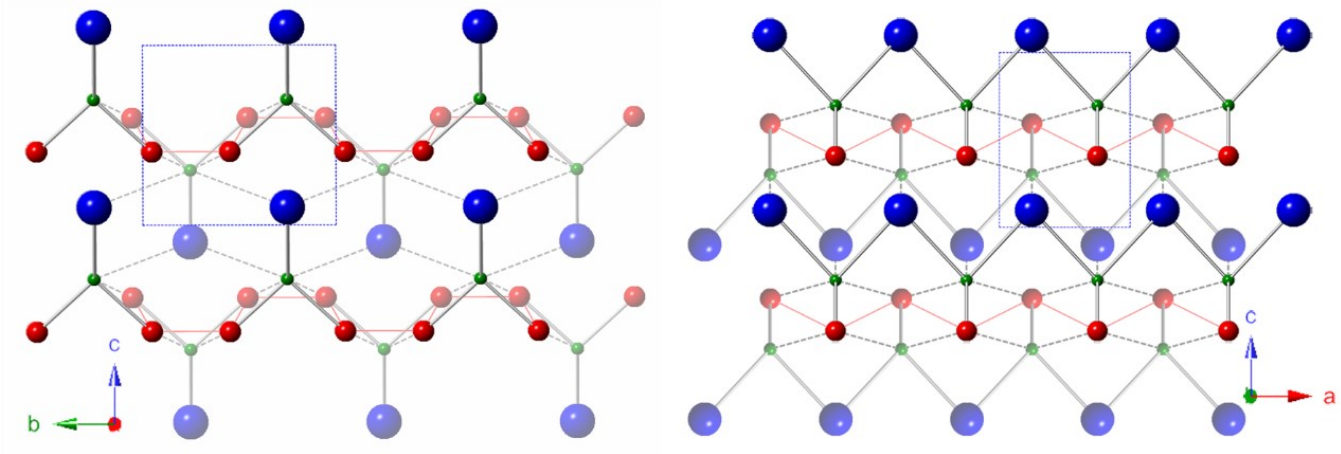

Figure 1. Schematic representation of the orthorhombic $AELi_2Ge$ structure, viewed along the crystallographic *a*-axis (left) and *b*-axis (right). *AE* atoms are represented as blue spheres, Ge atoms are drawn as green spheres, and Li atoms are shown with the red spheres. The "Ba2Li2Ge tetrahedral chains" are shown with atom connected by sticks; the inter-chain interactions are illustrated by the dash lines, and the Li—Li interactions are depicted with the thin red lines. The unit cell is outlined by the blue frame in both projections.

The crystal structure of $AELi_2Ge$ (*AE* = Ca, Sr, Ba) is schematically illustrated in Figure 1. The structure is formally assigned as belonging to the $BaLi_2Si$ type (Pearson symbol *oP*8) with space group *Pmmn* (no. 59). One way to look at the structure of $AELi_2Ge$ is to consider tetrahedral chains forming along *a* axis; the construction of these chains requires drawing bonds between Li and *AE* to nearest Ge atoms. Such chains are also coupled with two neighboring chains along *b* axis through Li—Li and Ge—Li interactions, which as judged by the interatomic distances must have appreciable covalent character. Taking into an account only these linked chains yields a layered structure, while including the various *AE*—Ge or *AE*—Li interactions between neighboring layers results into a 3D-like formation, depending on the nature of *AE*. According to the refined distances listed in Table 3, the Ca—Ge distance (3.1162(17) Å) is shorter than Ca—Li distance (3.2367(9) Å) and the Ba—Ge distance (3.4503(4) Å) between nearest neighbors is longer than the contact Ba—Li (3.4023(3) Å).

Table 3. Selected Interatomic Distances in $AELi_2Ge$ (*AE* = Ca, Sr, Ba).

Atomic pair	**Distance (Å)**	**Atomic pair**	**Distance (Å)**	**Atomic pair**	**Distance (Å)**
$CaLi_2Ge$		$SrLi_2Ge$		$BaLi_2Ge$	

Ge—Ca (×2)	3.117(2)	Ge—Sr (×2)	3.2891(4)	Ge—Ba (×2)	3.4503(4)
Ge—Ca (×2)	3.127(2)	Ge—Sr (×2)	3.3623(3)	Ge—Ba (×2)	3.6166(4)
Ge—Li (×2)	2.701(9)	Ge—Li (×2)	2.700(4)	Ge—Li (×2)	2.7228(2)
Ge—Li (×4)	2.808(2)	Ge—Li (×4)	2.803(2)	Ge—Li (×2)	2.7981(2)
Li—Li (×1)	2.59(1)	Li—Li (×1)	2.677(8)	Li—Li (×2)	2.7120(2)
Li—Li (×2)	2.678(9)	Li—Li (×2)	2.692(3)	Li—Li (×1)	3.7267(4)
Ca—Li (×2)	3.237(9)	Sr—Li (×2)	3.353(4)	Ba—Li (×2)	3.4023(3)

The structure under consideration can also be characterized as the intergrowth of two slabs: 1) "*AE*Ge" (PbO-like motif) and 2) "Li" slab, as shown in Figure 2. The slab "Li" is just a cutout from the hexagonally-close-packed structure of Li metal. This allows the present structure to be regarded as a "Li-intercalated" *AE*Ge phase, although in reality, the structures of the alkaline-earth monogermanides are different. Nonetheless, this analogy can useful if *AE*Ge are to be treated as electrodes in LIB.

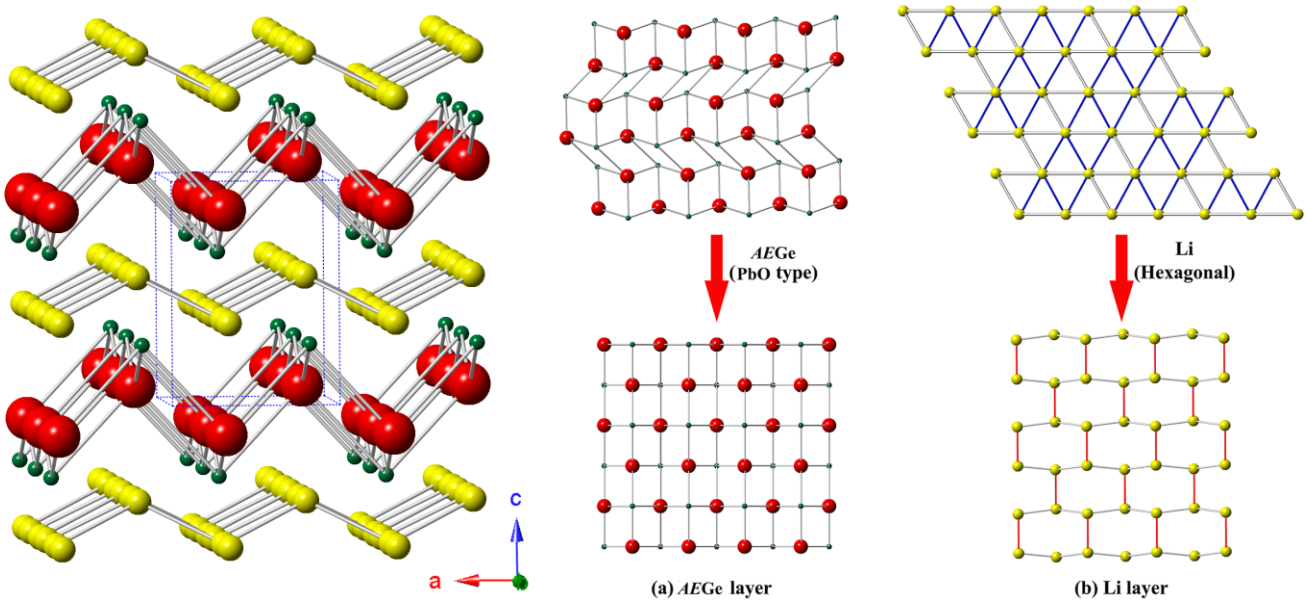

Figure 2. Schematic representation of $AELi_2Ge$, viewed approximately along the crystallographic b-axis and the projection of the crystal structure of $AELi_2Ge$ on the (001) planes: (a) *AE*Ge layer and (b) Li layer. *AE* atoms are represented as blue spheres, Ge atoms are drawn as green spheres, and Li atoms are shown with the red spheres. Both layers can be considered as the distortion of the corresponding simple compounds: (a) PbO-type *AE*Ge and (b) hexagonal Li.

In the $BaLi_2Ge$ structure, the shortest Ba—Ge distance is 3.4505(6) Å, close to the values seen in other Ba-Ge and Ba-Li-Ge compounds: $BaGe_2$ (3.42 Å) [39], $BaLiGe_2$ (3.37) Å) [40], Ba_2LiGe_3 (3.42 Å) [41,42], $Ba_8Li_5Ge_{41}$ (3.42 Å) [43], while the second shortest Ba—Ge distance 3.62 Å is larger

than these typical values, indicative of the weaker interactions between layers. In contrast, the shortest Li—Ge distance (2.72 Å) is close to the second shortest Li—Ge distance (2.80 Å). Both Li—Ge distances are longer than those in many ternary compounds: $BaLiGe_2$ (2.70 Å) [40], Ba_2LiGe_3 (2.58 Å) [41,42], $RE_3Li_4Ge_4$ (2.62 – 2.69 Å) [44] and $RE_2Li_2Ge_3$ (2.56 – 2.62) Å) [44], but close to the values reported for some ternary compounds such as LiZnGe (2.78 Å) [45]. Such longer Li—Ge distances suggest enhanced metallic characters compared with the reported alkaline-earth metal lithium germanides and rare-earth metal lithium germanides. The implied lesser covalency allows the valence electrons to be shared in multi-center interactions to stabilize the structure.

To better understand the nature of the Li—Ge bonding in $BaLi_2Ge$, the electronic density $\rho(r)$ maps were obtained by maximum enthropy method (MEM) analysis using the refined structure factors. As shown in Figure 3a, there are still electrons between Ge and the nearest Li and both atoms are elongated towards each other, indicating the strong covalent character and electron transfer. However, the shared or transferred electrons are not distributed exactly along the Li—Ge bond path, but curved toward to the second nearest Li atom to the Ge atom, suggestive of appreciable Li—Li bond/interactions to exist.

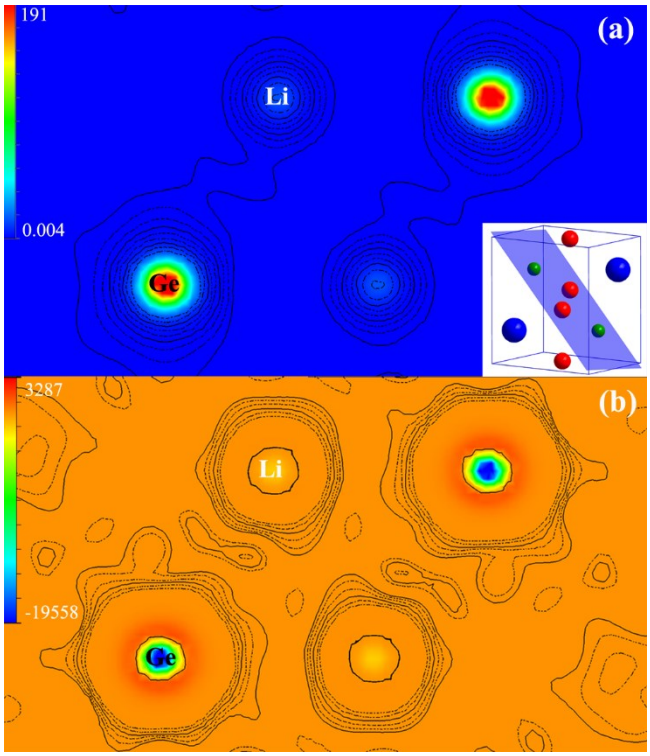

Figure 3. Electron density distributions obtained by MEM (a) and its Laplacian transformation (b). The inset crystallographic structure in (a) shows the crystal planes containing only Ge (green spheres) and Li (red spheres) atoms corresponding to the electron density distributions. The unit for the electronic density is e/Å^3. The logarithmic contour lines show 8 levels from minimum to the maximum.

Compared with the $\rho(r)$ map, its Laplacian function $L(r) = -\nabla^2\rho(r)$is more sensitive to the bond formation. When a chemical bond is formed, the $L(r)$ distribution is no longer spherical and its properties are widely used for characterizing atomic interactions, since the Laplacian enhances the features of charge distribution and of electron pair localization. The Li—Li bonding character is more evident in the Laplacian of the electron density, as shown by the distortion towards each other in Figure 3b.

3.2. Electronic Structure

Computations based on the density functional theory were carried out for $BaLi_2Ge$ with experimentally determined structural data. The Brillouin zone (BZ) is schematically illustrated in Figure 4 (the left side) with high symmetric *K* points to generate the band structure. The band structure and corresponding electronic density of states (DOS) are given in the middle and right of Figure 4. There are 8 energy bands in the range –10 eV to Fermi level (E_F) for valence electrons. Except two flat bands between –8 eV and –7 eV, six curved bands are in an energy range from –5 eV to the E_F, and these bands are degenerated into 3 energy levels in most zones of the BZ zone. These characters indicate the strong hybridization in the structure. The charge balance suggests the compound as a Zintl phase, but the hybridization in the Γ–Z zone elevates the energy of the filled band just below the Fermi level and reduces the energy of the empty band just above the Fermi level. As a result, the overlap of two bands leads to the DOS at Fermi level. The Fermi level located at the bottom of the valley in the total DOS, suggestive of an overall electronic structure stability (and likely poor metallic behavior). It is evident from the band structure that the DOS at Fermi level is mainly from the Γ–Z zone around Z (0, 0, k_z/2) point. It corresponds to the crystal planes parallel to (001) in the real space and suggests the metallic behaviors from delocalized electrons inside layers.

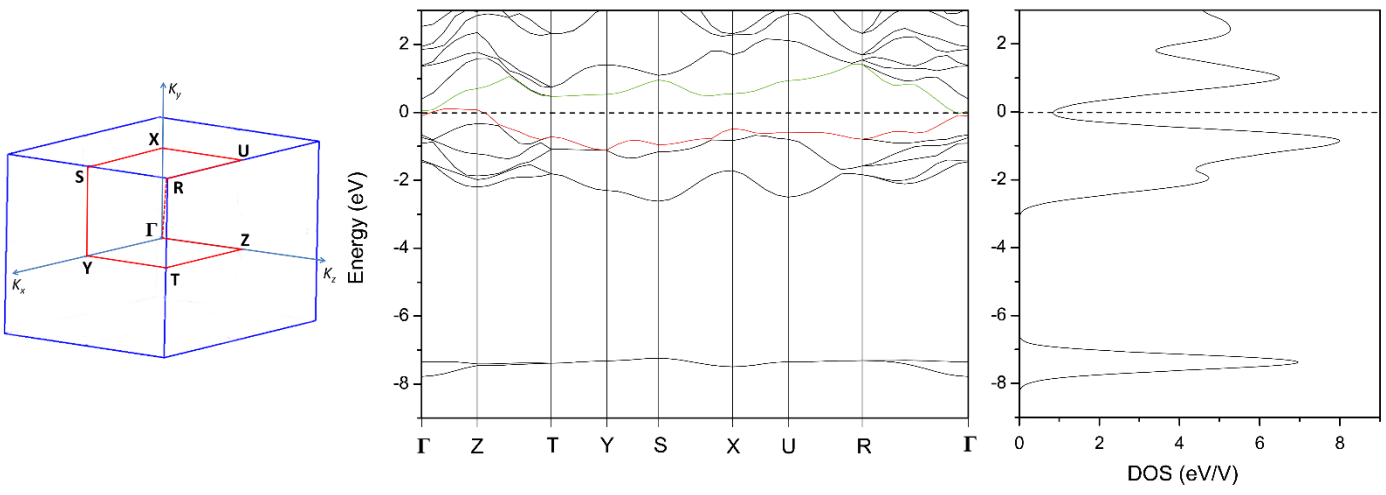

Figure 4. Band structure (middle) and DOS (right) of $BaLi_2Ge$, together with the schematically depicted Brillouin zone (left). The Fermi level is shown as the dash line. The red line in the band structure represents the main conductive band.

According to the partial DOS in Figure 5, strong hybridization of Ba-5*d* and Ge-3*p* states dominate the conduction band in the vicinity of the Fermi level E_F; this is inferred by their high DOS and similar distributions. Together with the band structure and total DOS in Figure 4, it can be inferred that the metallic behavior is associated the hybridization in BaGe layers. The DOS integration on the conduction band indicates the electron transfer of ca. 0.9 e from Li to Ge per unit cell. Together with the intergrowth conceptual description we gave earlier, the dominant bonding interactions can be summarized as follows: strong Ba—Ge interactions (5*d*–3*p* hybridization) favor the formation of Ba—Ge layer, while the interaction between Li and layer show more ionic characters, like Li intercalated graphite in rechargeable lithium ion battery [1,2].

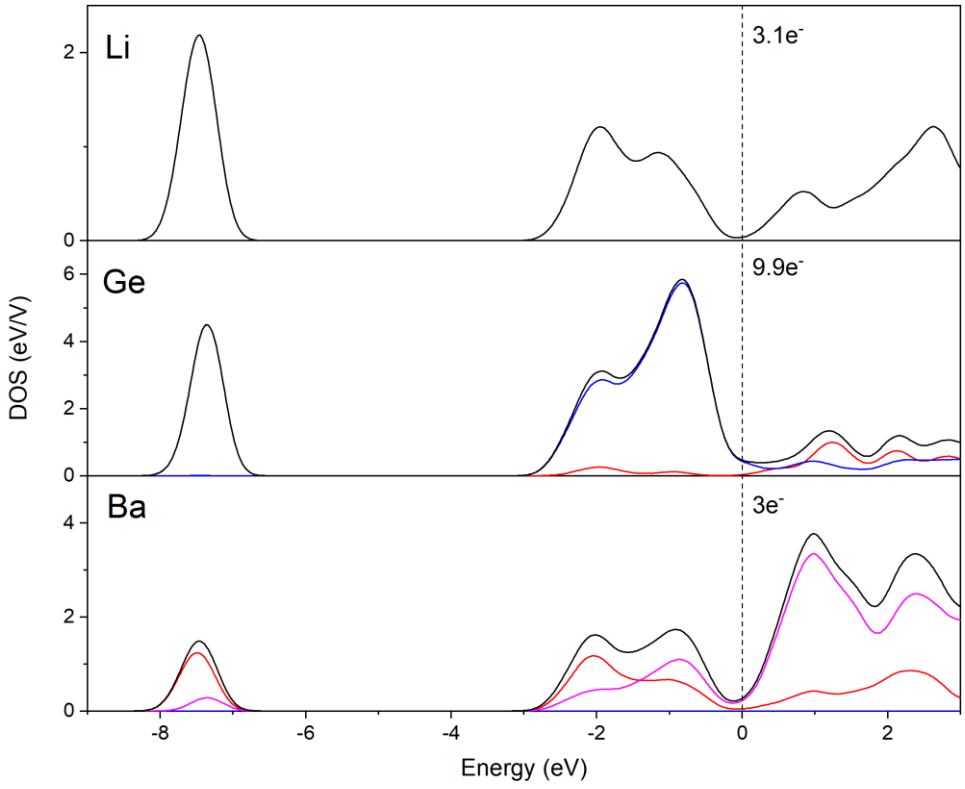

Figure 5. Partial DOS (black lines) for Ba, Li and Ge in $BaLi_2Ge$. Contributions from s-, p-, d- bands are shown by the blue, red and pink lines respectively. The dotted lines indicate the Fermi level. Around 0.9 electrons are transferred from Li to Ge (in one unit cell with two formula units).

3.3. Electrochemical Properties

According to the above discussion, the presented $AELi_2Ge$ (*AE* = Ca, Sr, Ba) compounds can suggested as potential electrodes for rechargeable LIB, following the delithiation/lithiation mechanism:

$$AELi_2Ge \rightarrow 2\times Li + 2\times e^- + AEGe$$

The theoretical capacity (C_{theor}) can be estimated using the following equation [46]:

$$C_{theor} = nF/3.6\times M$$

where n is the maximum number of charges of the compound can accept (or give up), F is Faraday's constant, and M is the formula weight of the compound in g/mol. From the above, CaGe has a C_{theor} of ca. 480 mAh/g.

Because of air sensitivity of finely ground powders of $CaLi_2Ge$, the electrochemical measurements were performed on CaGe electrodes, and the $CaLi_2Ge$ is the expected product of full lithiation. The cycling properties were measured in a current density of 50 mA/g, and shown in Figure 6. The initial discharge capacity (lithiation) is 446 mAh/g, close to the theoretical value, and the charge capacity in the first cycle is 225 mAh/g, which increases up to ca. 245 mAh/g in the following cycles. No visible capacity fading and high Coulombic efficiency up to 99% in the following 20 cycles suggest the intercalation nature of the electrochemical reaction.

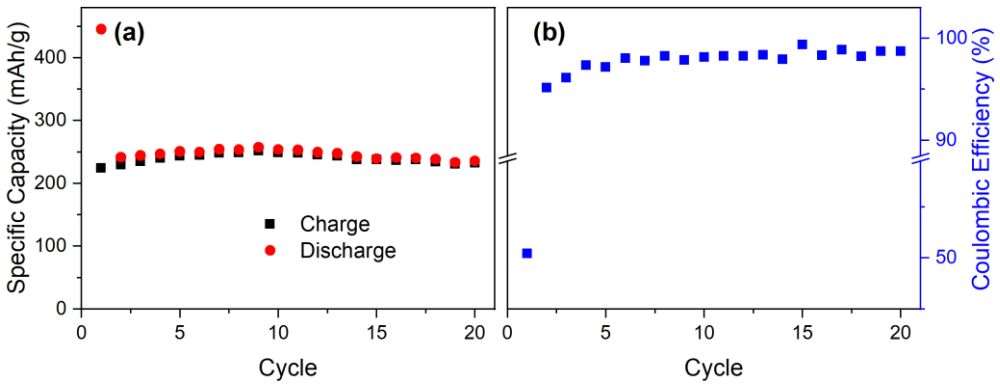

Figure 6. The electrochemical performance of polycrystalline CaGe. Panel (a) shows the specific capacity and panel (b) depicts the Coulombic efficiency.

The discharge capacity close to the theoretical value in the first cycle indicates the formation of $CaLi_2Ge$ via electrochemical intercalation. The charge capacity has only a half of the theoretical values suggests only one Li delithiated out from $CaLi_2Ge$. Thus the electrochemical reaction after the first cycle is likely $CaLi_2Ge \rightarrow Li + e^- + CaLiGe$. To confirm it, the ex situ PXRD was collected on the electrodes after 1st discharge-charge cycle. As

shown in Figure S1, after the 1st cycle, the main phase in the electrode is not CaGe but an unknown phase, except the Cu collector. Due to poor crystallinity, it is impossible to index the PXRD pattern. However, based on the electrochemical behaviors, it can be inferred that the phase has a formula CaLiGe or close to it, but the structure and existence of this phase remains to be confirmed in future works.

Author Contributions: Conceptualization, S.B.; methodology, J.Z.; S.B.; data curation, J.Z.; S.B.; validation, J.Z.; S.B.; formal analysis, J.Z.; S.B.; investigation, J.Z.; resources, S.B.; writing—original draft preparation, J.Z.; writing—conceptualization, J.Z.; S.B.; writing—review and editing, S.B.; visualization, S.B.; supervision, S.B.; project administration, S.B.; funding acquisition, S.B. All authors have read and agreed to the published version of the manuscript.

Funding: This work was supported by the US National Science Foundation (NSF) through grant DMR-2004579.

Data Availability Statement: The corresponding crystallographic information files (CIF) have been deposited with the Cambridge Crystallographic Database Centre (CCDC) and can be obtained free of charge via http://www.ccdc.cam.ac.uk/conts/retrieving.html (or from the CCDC, 12 Union Road, Cambridge CB2 1EZ, UK; Fax: +44-1223-336033; E-mail: deposit@ccdc.cam.ac.uk) with the following depository numbers: 2314734–2314736.

Acknowledgments: In this section, you can acknowledge any support given which is not covered by the author contribution or funding sections. This may include administrative and technical support, or donations in kind (e.g., materials used for experiments).

Conflicts of Interest: The authors declare no conflict of interest.

Appendix A

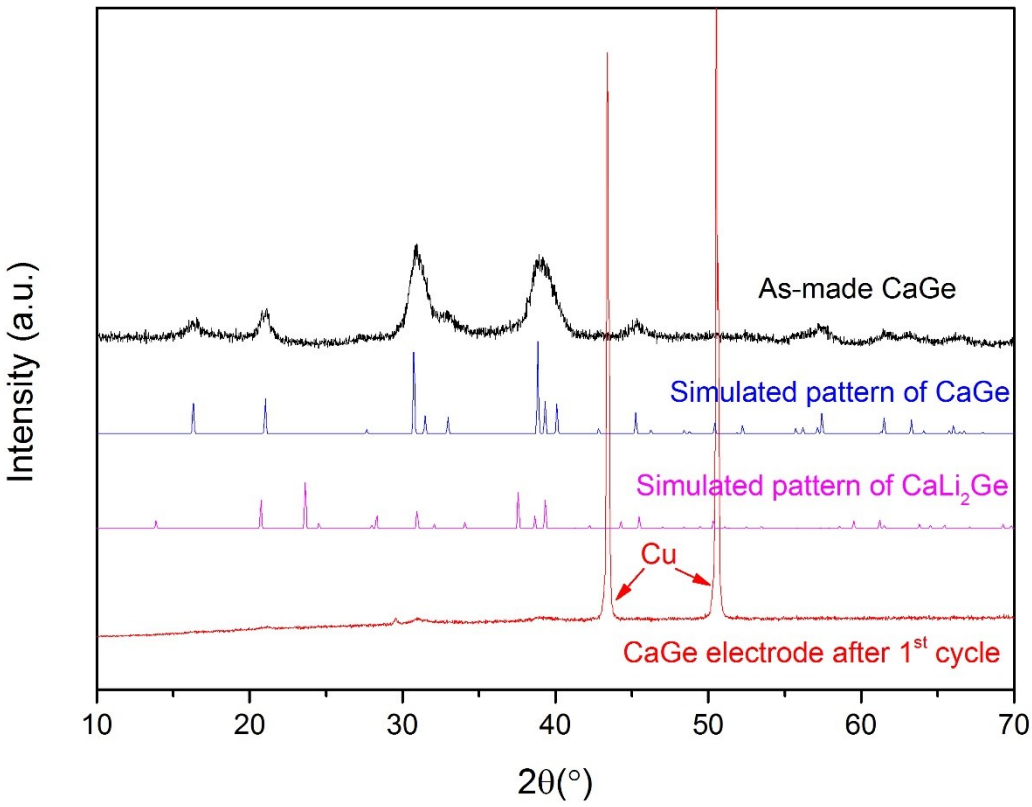

Figure A1. Powder X-ray diffraction patterns of as-made CaGe [CaGe powders were prepared via high energy ball milling using Ca (Aldrich, >99.9%) and Ge powders (Aldrich, >99.9%). The molar ratio of Ca and Ge was 1:1 with the total weight of 2 g. Stainless steel balls of 40 g were used and the ball milling was carried out under an Ar atmosphere for 3 hours] and CaGe electrodes after the first discharge-charge cycle, together with simulated patterns of CaGe and $CaLi_2Ge$. A small sharp peak appears at ca. 30º n the pattern of CaGe electrode after the first cycle, and it does not match a known phase.

References

1. Whittingham, M.S.; Lithium Batteries and Cathode Materials. *Chem. Rev.* **2004**, *104*, 4271-4301.
2. Goodenough, J.B.; Park, K.S.; The Li-Ion Rechargeable Battery: A Perspective. *J. Am. Chem. Soc.* **2013**, *135*, 1167-1176.
3. Goodenough, J.B.; Kim, Y.; Challenges for Rechargeable Li Batteries. *Chem. Mater.* **2010**, *22*, 587-603.
4. Sathiya, M; Rousse, G.; Ramesha, K.; Laisa, C.P.; Vezin, H.; Sougrati, M.T.; Doublet, M.L.; Foix, D.; Gonbeau, D.; Walker, W.; Prakash, A.S.; Ben Hassine, M.; Doupont, L.; Tarascon, J.M.; Reversible Anionic Redox Chemistry in High-Capacity Layered-Oxide Electrodes. *Nat. Mater.* **2013**, *12*, 827-835.
5. Goodenough, J.B.; Evolution of Strategies for Modern Rechargeable Batteries. *Acc. Chem. Res*. **2013**, *46*, 1053-1046.
6. Lee, J.; Urban, A.; Li, X.; Su, D.; Hautier, G.; Ceder, G.; *Science* **2014**, *343*, 519.
7. Collins, C.; Dyer, M.S.; Pitcher, M.J.; Whitehead, G.F.S.; Zanella, M.; Mandal, P; Claridge, J.B.; Darling, G.R.; Rosseinsky, M.J.; Accelerated Discovery of Two Crystal Structure Types in a Complex Inorganic Phase Field. Nature **2017**, *546*, 280.
8. Dyer, M.S.; Collins, C.; Hodgeman, D.; Chater, P.A.; Demont, A.; Romani, S.; Sayer, R.; Thomas, M.F.; Claridge, J.B.; Darling, G.R.; Rosseinsky, M.J.; Computationally Assisted Identification of Functional Inorganic Materials. *Science* **2013**, *340*, 847-852.

9. Longo, R.C.; Kong, F.T.; Santosh, K.C.; Park, M.S.; Yoon, J.; Yeon, D.H.; Park, J.H.; Doo, S.G.; Cho, K.; Phase Stability of Li-Mn-O Oxides as Cathode Materials for Li-ion Batteries: Insights from Ab Initio Calculation. *Phys. Chem. Chem. Phys.* **2014**, *16*, 11218.
10. Matsuno, S.; Noji, M.; Kashiwagi, T.; Nakayama, M.; Wakihara, M; Construction of the Ternary Phase Diagram for the Li-Cu-Sb System as the Anode Materials for a Lithium Ion Battery. *J. Phys. Chem. C* **2007**, *111*, 7548-7553.
11. Massalski, T.B., Ed,; Binary Alloys Phase Diagrams; ASM International: Materials Park, OH, 1990.
12. St. John, M.R.; Furgala, A.J.; Sammells, A.F.; Thermodynamic Studies of Li-Ge Alloys: Application to Negative Electrodes for Molten Salt Batteries. *J. Electrochem. Soc.* **1982**, *129*, 246-150.
13. Vhof, V.; Muller, W.; Schafer, H.; The Structure of Li_7Ge_2. *Z. Naturforsch. B* **1972**, *27B*, 1157-1160.
14. Fassler, T.F.; Zeilinger, M.; Structural and Thermodynamic Similarities of Phases in the Li-*Tt* (*Tt* = Si, Ge) Systems: Redetermination of the Lithium-rich Side of the Li-Ge Phase Diagram and Crystal Structure of $Li_{17}Si_{4-x}Ge_x$ for x = 2.3, 3.1, 3.5 and 4 As Well As $Li_{4.1}Ge$. *Dalton Trans.* **2014**, *43*, 14959-14970.
15. (a) Johnson, Q.; Smith G.S.; Wood, D.; The Crystal Structure of $Li_{15}Ge_4$. *Acta Crystallogr.* **1965**, *18*, 131-132; (b) Osman, H. H.; Bobev, S.; Experimental and Theoretical Study on the Substitution Patterns in Lithium Germanides: The Case of $Li_{15}Ge_4$ vs $Li_{14}ZnGe_4$ *Eur. J. Inorg. Chem.* **2022**, e202100901.
16. Goward, G.R.; Taylor, N.J.; Souza, D.C.S.; Nazar, L.; The True Crystal Structure of $Li_{17}M_4$ (*M* = Ge, Sn, Pb) – Revised from $Li_{22}M_5$. *J. Alloys Compd.* **2001**, *329*, 82-91.
17. Tillard, M.; Belin, C.; Spina, L.; Jia, Y.Z.; Two Cubic Polymorphs of AlGeLi. Acta Crystallogr. Sect. C 2012, 68, i60-i64.
18. Henze, A.; Hlukhyy, V.; Fassler, T.F.; Fully and Partially Li-Stuffed Diamond Polytypes with Ag-Ge Structures: Li_2AgGe and $Li_{2.53}AgGe_2$. *Inorg. Chem.* **2015**, *54*, 1152-1158.
19. Todorov, I.; Sevov, S.C.; Heavy-Metal Aromatic and Conjugated Species: Rings, Oligomers, and Chains of Tin in $Li_{9-x}EuSn_{6+x}$, $Li_{9-x}CaSn_{6+x}$, $Li_5Ca_7Sn_{11}$, $Li_6Eu_5Sn_9$, $LiMgEu_2Sn_3$, and $LiMgSr_2Sn_3$. *Inorg. Chem.* **2005**, *44*, 5361-5369
20. Ganguli, A.K.; Gupta, S.; Corbett, J.D.; New Tetragonal Structure Type for $A_2Ca_{10}Sb_9$ (*A* = Li, Mg). Electronic Variability Around a Zintl Phase. *Inorg. Chem.* **2006**, *45*, 196-200.
21. Stegmaier, S.; Waibel, M.; Henze, A.; Jantke, L.A.; Karttunen, A.J.; Fassler, T.F.; Soluble Zintl phase $A_{14}ZnGe_{16}$ (*A* = K, Rb) Featuring $[(\eta^3\text{-}Ge_4)Zn(\eta^3\text{-}Ge_4)]^{6-}$ and $[Ge_4]^{4-}$ Clusters and the Isolation of $[(MesCu)_2(\eta^3\text{-}Ge_4)Zn(\eta^3,\eta^3\text{-}Ge_4)]^{4-}$: The Missing Link in the Solution Chemistry of Tetrahedral Group 14 Element Zintl Clusters. *J. Am. Chem. Soc.* **2012**, *134*, 14450-14460.
22. Luo, X.H.; krizan, J.W.; Haldolaarachchige, N.; Klimczuk, T.; Xiw, W.W.; Fuccillo, M.K., Felser, C.; Cava, R.J.; A Large Family of Filled Skutterudites Stabilized by Electron Count. *Nat. Commun.* **2015**, *6*, 6489.
23. Schafer M.C.; Bobev, S.; Tin Clathrates with the Type II Structure. *J. Am. Chem. Soc.* **2013**, *135*, 1696.
24. Fassler, T.F. (ed.); Zintl Ions: Principles and Recent Developments. Springer-Verlag Berlin Heidelberg 2011.
25. Stoiber, D.; Bobnar, M.; Hohn, P.; Niewa, R.; Lithium Alkaline Earth Tetrelides of the type Li_2AeTt (*Ae* = Ca, Ba, *Tt* = Si, Ge, Sn, Pb): Synthesis, Crystal Structures and Physical Properties. *Z. Naturforsch. B* **2017**, *72*, 220-222.
26. SMART NT, version 5.63; Bruker Analytical X-ray Systems, In.: Madison , WI, 2003.
27. SAINT NT, version 6.45; Bruker Analytical X-ray Systems, In.; Madison, WI, 2003.
28. SADABS NT, version 2.10; Bruker Analytical X-ray Systems, In.; Madison, WI, 2001.
29. SHELXTL, version 6.12; Bruker Analytical X-ray Systems, In.; Madison, WI, 2001.
30. Momma, K.; Ikeda, T.; Belik, A.A.; Izumi, F.; Dysnomia, A Computer Program for Maximum-Entropy Method (MEM) Analysis and its Performance in the MEM-based Pattern Fitting. *Powder Diffr.* **2013**, *28*, 184-193.
31. Momma, K.; Izumi, F.; VESTA 3 for Three-Dimensional Visualization of Crystal, Volumetric and Morphology Data. *J. Appl. Cryst.* **2011**, *44*, 1272-1276.
32. Ordejón, P.; Artacho, E.; Soler, J.M. Self-consistent Order-N Density-Functional Calculations for Very Large Systems. *Phys. Rev. B* **1996**, *53*, R10441.
33. Soler, J.M.; Artacho, E.; Gale, J.D.; García, A.; Junquera, J.; Ordejón, P.; Sánchez-Portal, D. The SIESTA Method for Ab Initio Order-N Materials Simulation. *J. Phys.: Condens. Matter* **2002**, *14*, 2745.
34. Troullier, N.; Martins, J.L. Efficient Pseudopotentials for Plane-Wave Calculations. *Phys. Rev. B* **1991**, *43*, 1993.
35. Perdew, J.P.; Burke, K.; Emzerhof, M. Generalized Gradient Approximation Made Simple. *Phys. Rev. Lett.* **1996**, *77*, 3865.
36. Kresse, G.; Hafner, J. Ab Initio Molecular Dynamics for Liquid Metals. *Phy. Rev. B* **1993**, *47*, 558.
37. Kresse, G.; Joubert, D. From Ultrasoft Pseudopotential to the Projector Augmented-Wave Method. *Phys. Rev. B* **1999**, *59*, 1758.
38. Von Narth, U.; Hedin, L.A. A Local Exchange-Correlation Potential for the Spin Polarized Case. I. *J. Phys. C* **1972**, *5*, 1629.
39. Betz, A.; Schafer, H.; Weiss, A.; Wulf, R.; Digermanide $SrGe_2$ and $BaGe_2$. *Z. Naturforsch. B* **1968**, *23*, 878.
40. Park, D.G.; Dong, Y.; DiSalvo, F.J.; $LiSrGe_2$ and $LiBaGe_2$: One-Dimensional Chains of $[Ge_2]^{3-}$ in an Unusual Conformation. *J. Alloys Compd.* **2009**, *470*, 90-95.
41. von Schnering, H.G.; Bolle, U.; Curde, J.; Peter, K.; Carillo-Cabrera, W.; Mehmet, S.; Schultheiss, M.; Wedig, U.; Hucker Arenes with Ten π Electrons: Cyclic Zintl Anions $[Si_6]^{10-}$ and $[Ge_6]^{10-}$, Isosteric with $[P6]^{4-}$. *Angew. Chem.* **1996**, *35*, 984-986
42. Ghosh, K.; Bobev, S.; Yet Another Case of Lithium Metal Atoms and Germanium Atoms Sharing Chemistry in the Solid State: Synthesis and Structural Characterization of Ba_2LiGe_3. *Chem. Eur. J.* **2023**, *29*, e202302385.

43. Ghosh, K.; Ovchinnikov, A.; Baitinger, M.; Krnel, M.; Burkhardt, U.; Grin, Y.; Bobev, S.; Lithium Metal Atoms Fill Vacancies in the Germanium Network of a Type-I Clathrate: Synthesis and Structural Characterization of $Ba_8Li_5Ge_{41}$. *Dalton Trans.* **2023**, *52*, 10310.
44. Guo, S.P.; You, T.S.; Bobev, S.; Closely Related Rare-Earth Metal Germanides $RE_2Li_2Ge_3$ and $RE_3Li_4Ge_4$ (*RE*=La-Nd, Sm): Synthesis, Crystal Chemistry, and Magnetic Properties. *Inorg. Chem.* **2012**, *51*, 3119-3129.
45. Lacroix-Orio, L.; Tillard, M.; Belin, C.; Synthesis, Crystal and Electronic Structure of $Li_8Zn_2Ge_3$, a Compound Displaying an Open Layered Anionic Network. *Solid State Sci.* **2006**, *8*, 208-215.
46. Howard, W.F.; Spotnitz, R.M.; Theoretical Evaluation of High-Energy Lithium Metal Phosphate Cathode Materials in Li-ion Batteries. *J. Power Source* **2007**, *165*, 887.